Advances in Materials Technology for Fossil Power Plants
Proceedings from the Seventh International Conference
October 22–25, 2013, Waikoloa, Hawaii, USA
https://doi.org/10.31399/asm.cp.am-epri-2013p1038

D. Gandy, J. Shingledecker, editors

MODELING A STRESS RELAXATION CRACKING TEST FOR ADVANCED ULTRA SUPERCRITICAL ALLOYS

David C. Tung and John C. Lippold
The Ohio State University

ABSTRACT

Finite element (FE) modeling has been applied to a stress relaxation cracking (SRC) test in order to evaluate the effects of changing sample geometry and material type. This SRC test uses compressive pre-straining to create a tensile residual stress in modified compact-tension specimens and has been used to test 316H stainless steel. The FE model is first used to verify that sample integrity will not be compromised by modifying the geometry. The FE model is then applied to candidate Advanced Ultra Supercritical nickel-base alloys 617, 740H, and 800. It is determined that this stress relaxation test will be appropriate for these alloys.

INTRODUCTION

INCONEL® Alloy 740H, a candidate superalloy for Advanced Ultra SuperCritical (AUSC) coal-fired power plant construction, has recently been the subject of considerable research [1-11]. Remaining research includes an investigation of stress relaxation cracking, a cracking phenomenon that raised concern during the development of Alloy 617 for the European AUSC program [12]. Stress relaxation cracking typically occurs in service after many thousands of hours (10,000 – 100,000 hours) and is, in general, due to the acceleration of creep by residual stress [13-16]. SRC is typically associated with the heat affected zone (HAZ) of welds but weld metal and regions of cold work are also susceptible [14, 17]. The thermal excursion associated with welding leads to the development of residual stress on cooling and also significantly affects the microstructure surrounding the weld. Strengthening precipitates (carbides or γ') dissolve in the HAZ and re-precipitate during heat treatment or service. The nature of this re-precipitation drives SRC. Typically, strengthening precipitates re-precipitate in grain interiors, strengthening them relative to the grain boundaries. This forces stress relaxation to be concentrated on grain boundaries. Additionally, carbide precipitation on grain boundaries can consume the alloying elements that might have formed strengthening precipitates near the boundary, further weakening grain boundaries and immediately surrounding areas. As a result of this precipitate distribution, SRC typically occurs intergranularly [14, 16-18].

While the terms stress relaxation cracking and strain age cracking (SAC) are often used interchangeably and their mechanisms are similar, there is one major difference which merits discussion. Unlike stress relaxation cracking, strain age cracking primarily occurs in superalloys which harden very rapidly during aging. Due to this rapid hardening, SAC typically occurs during heating or aging. The time required for SAC to occur is very short, especially when compared to the thousands of hours required for SRC to occur and this is the main difference between SAC and SRC. If it is not possible to heat large components to a stress relieving temperature quickly enough, SAC will be very difficult to avoid. It is often necessary to use alloys that harden slowly (e.g. 718) for welded construction in order to avoid strain age cracking. Stress relaxation cracking occurs after much longer times and can be avoided with stress relieving heat treatments because heating rate is less critical.

Since alloys which harden very rapidly will crack due to SAC before reaching service, their SRC susceptibility is somewhat irrelevant but alloys which can be aged without cracking are not susceptible to SAC but may still be susceptible SRC. While this distinction is minor, it should be kept in mind that SAC tests, which are meant to reveal failures that occur in a short time, will be less useful when evaluating susceptibility to long-term cracking mechanisms such as SRC.

The long-term nature of SRC and the large time window within which it may occur make it very difficult to predict and therefore it is particularly concerning. There are many different approaches to SRC testing and most of them rely on an externally applied load to generate cracking. A detailed explanation of many of these tests can be found in the SRC reviews by Siefert and Tanzosh [14] and Dhooge and Vinckier [18]. Self-restrained testing approaches include the Borland test [19] and compressively pre-strained compact tension specimens [13, 15]. Compressively pre-strained compact tension specimens are particularly interesting because they have been well characterized in the recent past, and are easy to model, fabricate, and inspect. Recent work has been done with this type of test examining SRC in 316H stainless steel [15]. In this work, Turski, et al. accurately modeled the stress state after pre-straining and accurately predicted the magnitude of damage due to SRC in a 4500 hour test. The aim of the present study is to determine the feasibility of applying such a test to alloy 740H and other Ni-base alloys using the finite element software Abaqus [20].

Alloys 617 and 800 were chosen for comparison with alloy 740H because they have both demonstrated susceptibility to SRC [12, 17]. Alloy 617 is an AUSC candidate alloy but lacks the high temperature strength of alloy 740H. This has consequences with respect to wall thickness, maximum pipe inner diameter, and other design parameters [1]. Alloy 800 is another nickel-base alloy that can demonstrate susceptibility to SRC and can be tested at a similar temperature as 617 and 740H. The compositions of these alloys are given in Table 1. Considering these compositions with respect to the mechanism of SRC explained earlier, 316H is susceptible due to its high carbon content. Alloys 617 and 800 have more carbon and are also hardened by a small amount of γ' and they are also susceptible to SRC. Alloy 740H, which has a similar carbon content as 316H, has the highest levels of γ' forming elements and therefore the strongest precipitation; however, it may not be the most SRC susceptible alloy because other factors such as creep ductility play an important role the SRC mechanism [14, 16].

Table 1. Nominal compositions of alloys in this study in weight percent. All values are maxima. Note that in alloy 740H, the 'H' does not indicate high carbon as it does in 316H.

	Ni	Cr	Co	Fe	Mo	Al	Ti	C
800 [21]	35	23	-	Bal	-	0.6	0.6	0.10
617 [22]	Bal	24	15	3	10	1.5	0.6	0.15
740H [23]	Bal	25	20	1.5	0.5	1.4	1.4	0.06
316H [16]	12	17	-	Bal	2.2	-	-	0.07

EXPERIMENTAL PROCEDURE

In order to evaluate the feasibility of using compressively pre-strained compact tension specimens, the first step was to create a finite element model that matches the work done by Turski, et al. [15]. This was done using alloy 316H. Once this model was established, it was used to evaluate a modified sample geometry. The sample geometry was modified in order to accommodate currently available material. The finite element model of the modified geometry was then used to evaluate alloys 740H, 617, and 800.

Following the work of Turski, et al., a 3D finite element model was created using the approximate dimensions, properties, and procedure given in their publication. The sample geometries used in this study is shown in Figure 1 below.

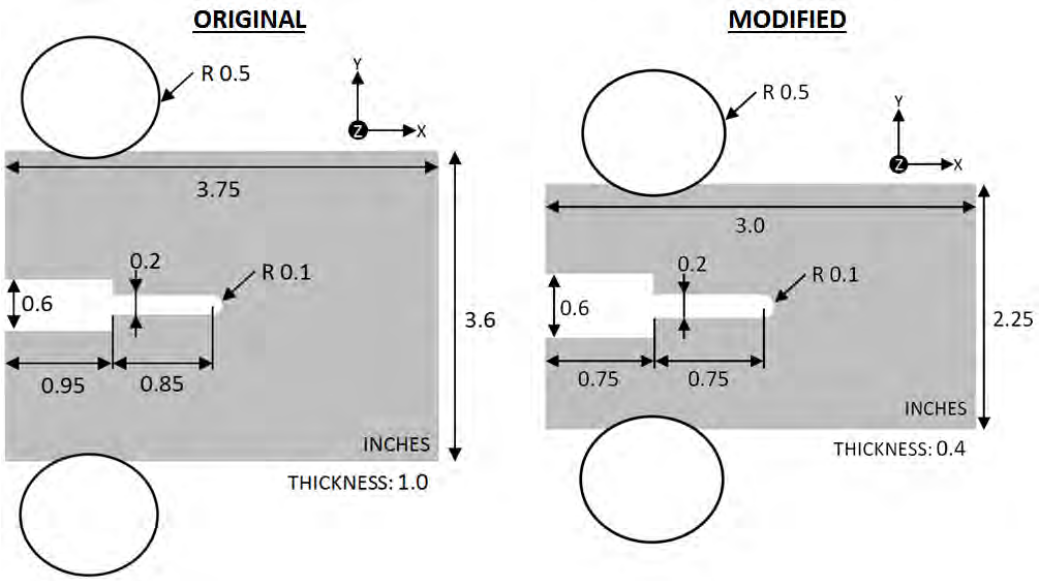

Figure 1. Sample geometries considered in this study. Note the different thicknesses.

Using the finite element software package Abaqus, rigid cylinders were used to compress a compact tension specimen 2 mm. The compression was applied to a full 3D model using boundary conditions to move each cylinder 1 mm towards each other. In order to observe residual stresses, the y-direction boundary conditions of the cylinders were removed and a remote portion of the sample was fixed. Residual stress and elastic strains in the crack opening direction (y-direction, S22, EE22) were recorded in order to compare with the results of Turski et al. Triaxiality was taken to be the negative ratio of hydrostatic pressure to Mises stress, as defined by Abaqus [24]. These three parameters were considered for a path along the mid-thickness and quarter-thickness planes immediately behind the notch root. These paths are shown in Figure 2.

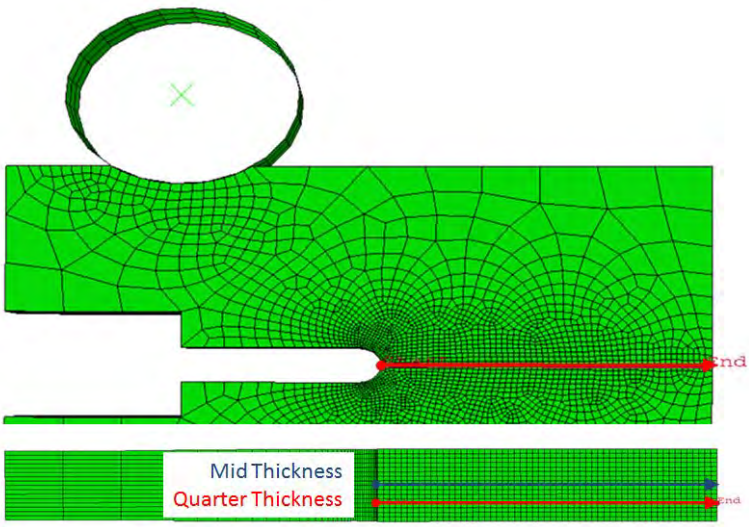

Figure 2. The paths used to query the model for data shown on a meshed model of the modified geometry.

Once a model that resembled the results of Turski, et al. was created, the geometry was modified to that in Figure 1 and the same parameters were considered again. Upon discovering that this modified geometry created a very similar stress state, it was used to consider alloys 740H, 617, and 800. The material property data used for these models are given in Table 2. Turski, et al. generated additional stress-strain data specifically for their study and this data were also used in the present work.

Table 2. Material property data used for modeling. A more thorough stress-strain profile was entered for 316H in the current study and the work by Turski, et al [15].

	316H [15]	Alloy 617 [22]	Alloy 740 [23] 800 °C / 16 h	Alloy 800H [21] hot rolled
	Mpa (ksi)	Mpa (ksi)	Mpa (ksi)	MPa (ksi)
E	204,000 (29,600)	211,000 (30,600)	221,000 (32,000)	196,500 (28,500)
ν	0.27	0.3	0.3	0.337
σ_y	250 (36.3)	322 (46.7)	720.5 (104.5)	445 (64.6)
σ_{UTS}	895 (129.8)	734 (109.5)	1169 (169.5)	665 (96.4)

RESULTS AND DISCUSSION

A model that produced results similar to those obtained by Turski, et al. [15] was created. The model was considered representative on the bases of residual stress and elastic strains in the crack opening direction. This direction is defined as the y-direction, the principal components along which are identified as “22”. The data generated with the present model and the data reported by Turski, et al. are compared in Figure 3 and Figure 4 below. It should be noted that Turski, et al. determined that isotropic hardening was the most appropriate based on elastic strain measurements, some of which are shown in Figure 4, so the current model also considers isotropic hardening.

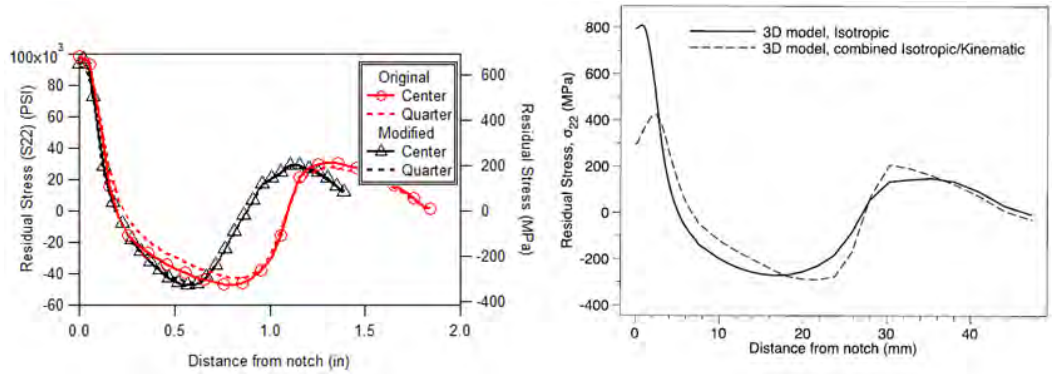

Figure 3. Comparison of crack-opening residual stresses. Data from Turski, et al. is on the right and data from the current work is on the left. Even though only the 'Original' geometry should be compared to the data from Turski, et al., there are strong similarities among all sets of data, especially within the first half inch.

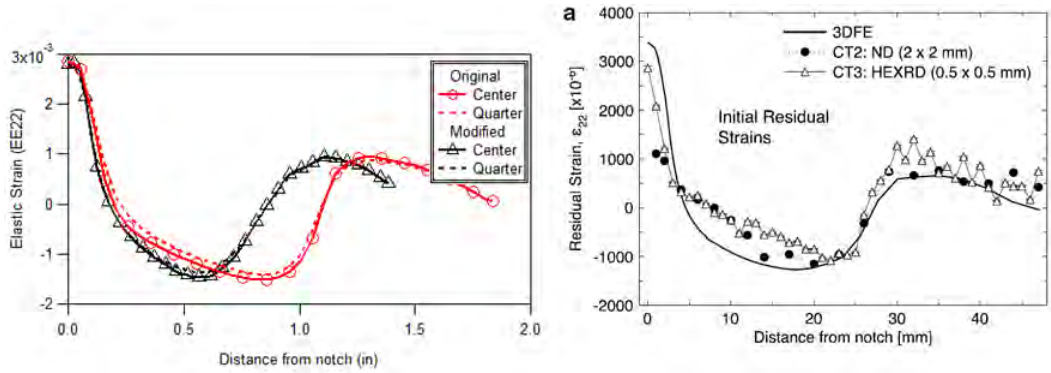

Figure 4. Comparison of elastic strain in the crack opening direction. Data from Turski, et al. is on the right and data from the current work is on the left. As with the residual stress data, very strong similarities can be seen, especially within the first half inch.

While the initial peaks are slightly smaller than the reported data [15], they are still rather comparable and the magnitude and position of the other maxima and minima are accurate. Some possible sources of error include an inexact duplication of the sample geometry and a different mesh shape. At this point it was determined that the present model was sufficient to continue the analysis.

After modifying the geometry in order to accommodate available material, residual stress, elastic strain, and triaxiality were compared between the two models on both the mid-thickness and quarter-thickness planes. Stress and strain data were shown above and triaxiality data is shown in Figure 5 below.

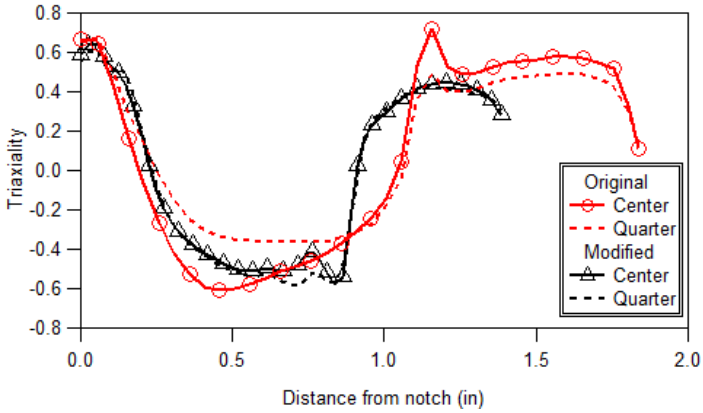

Figure 5. Triaxiality data for the original and modified sample geometries along both the mid- and quarter-thickness planes. As with the other data, good agreement can be seen, especially in the first half inch behind the notch.

These graphs indicate that the geometry modification did not significantly change the residual stress, elastic strain, or triaxiality, especially near the notch root. As expected, the profiles were shifted to be narrower in the modified sample since the sample itself was shortened. Another important point is that in both models, there are very minor differences between the mid-thickness and quarter-thickness profiles. This indicates that the profiles of these parameters are constant for at least half of the sample thickness in both geometries. The quarter thickness plane is particularly interesting because a somewhat constant depth of cracking was observed behind the notch between the mid-thickness and quarter-thickness planes [15]. The fractographs that report the cracking depth are shown in Figure 6. Based on the similarities of the magnitudes and breadths of these parameters, it was concluded that the modified sample geometry is thick enough to produce the same residual stress state that was observed by Turski, et al.

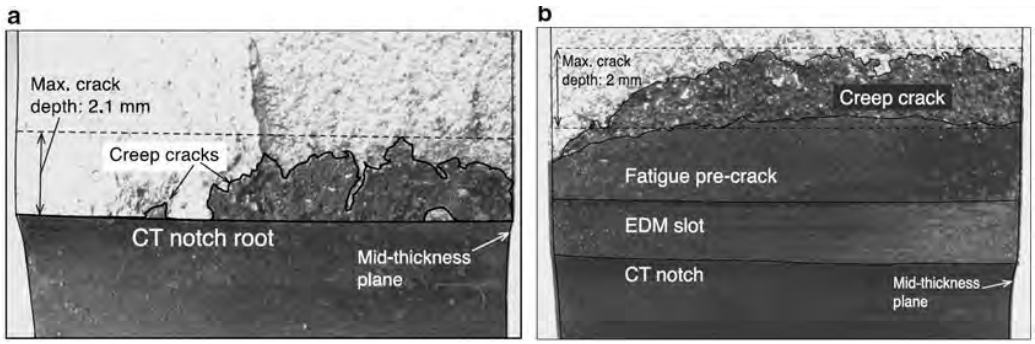

Figure 6. Fractographs from the work of Turski, et al. showing the depth of cracking behind the notch. Notice how the maximum crack depth is somewhat constant over at least half of the sample. Half of a 1 inch thick sample is shown here.

After accepting the modified geometry, other materials were modeled. The residual stress and elastic strain levels were variable which should be expected due to the dependence of these parameters on material properties. Triaxiality was found to be relatively comparable, especially near the notch root. This is also expected since triaxiality is a ratio of stresses and is therefore less subject to individual material properties. The slightly different profile for alloy 316H is likely due to the material property data entered into the model. Several points along the stress-strain curve were entered for only 316H because Turski, et al. specifically determined data for this purpose. It is expected that this increased the resolution of the model and provided a level of accuracy that

could not be achieved without such data. Residual stress, elastic strain, and triaxiality data are all graphed in Figure 7. Data from the quarter thickness plane was omitted because in every case it is very similar to the data from the mid-thickness plane.

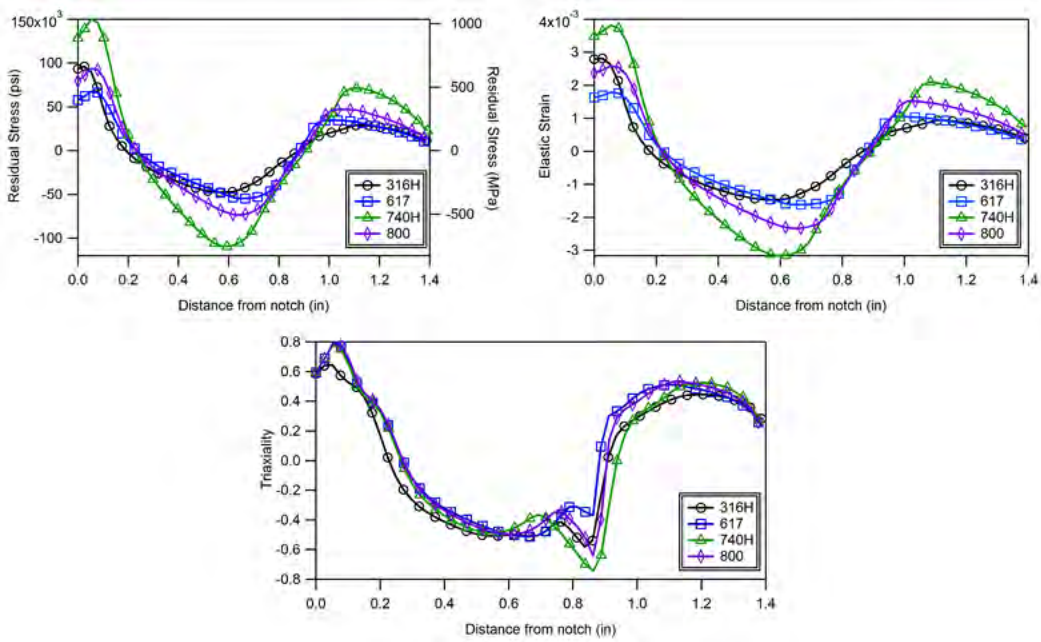

Figure 7. Comparison of residual stress, elastic strain, and triaxiality as modeled for the alloys in this study. Data is from the mid-thickness plane of the modified sample geometry.

While the similar levels of triaxiality indicate similar stress states, they do not describe the stress magnitude. In order to evaluate the magnitude of these residual stress levels, the peak residual stresses for each alloy were normalized by the stress required to cause rupture in 4000 hours at a temperature near 750 °C. A temperature closer to 550 °C was considered for 316H because this material was originally tested at 550 °C [15]. Rupture stress was chosen as the normalization parameter since SRC is so closely related to creep and a failure time of 4000 hours was chosen based on the experiments by Turski, et al. which were 4500 hours long. It was found that for all of the alloys studied here, the peak residual stress is approximately 4-7 times greater than the stress required to cause rupture in 4000 hours near 750 °C. The detailed data can be found in Table 3. Since these alloys all exhibit a very similar level of triaxiality and will all experience a similar residual stress level relative to their stress rupture strengths, it is concluded that such a test for SRC would provide a reasonable comparison between these alloys.

Table 3. Data used to evaluate the residual stress levels calculated by the FE model. All of the stresses correspond to failure after 4000 hours at the indicated temperature.

	316H [25]	Alloy 617 [22]	Alloy 740 [23] 800 °C / 16 h	Alloy 800H [21] annealed
	Mpa (ksi)	Mpa (ksi)	Mpa (ksi)	Mpa
T (C)	600	760	750	705
$\sigma_{Rupture}$	190 (27.5)	124 (18)	214 (31)	55 (8)
Max σ_{22}	800 (98.7)	649 (94.1)	1036 (150.2)	362 (52.5)
Max/Rupture	3.6	3.7	4.8	6.6

CONCLUSIONS

It is concluded that the sample geometry used by Turski, et al. can be modified to accommodate available material without significant penalties in residual stress state or magnitude. It is further concluded that the approach of compressively pre-straining compact tension specimens in order to produce a tensile residual stress will produce the same residual stress state and relative level in candidate AUSC nickel-base alloys. This tensile residual stress will be used to evaluate stress relaxation cracking susceptibility. In future work, alloy 740H samples will be subjected to thermal cycles before pre-straining in order to simulate an as-welded HAZ, postweld heat treated HAZ, and fully aged base metal microstructures. The SRC susceptibility of these microstructures will be compared to alloys 617 and 800, which are known to be susceptible to SRC.

ACKNOWLEDGEMENTS

The authors would like to thank Joe Dierksheide and Jim Tanzosh of Babcock and Wilcox for financial support, Brian Baker, Ronnie Gollihue, and Jack DeBarbadillo of Special Metals for material, and Professor Wei Zhang, Ryan Smith, and members of the OSU Welding and Joining Metallurgy Group for helpful discussions.

REFERENCES

[1] Baker, B.A., R.D. Gollihue, and J.J. deBarbadillo, *Fabrication and Heat Treatment of Weld Joints in Inconel Alloy 740H Superalloy Steam Header Pipe and Superheater Tubing*, in *Welding and Repair Technology for Power Plants: Tenth International EPRI Conference*, D. Gandy, Editor. 2012: Marco Island, FL.

[2] Evans, N.D., et al., *Microstructure and phase stability in INCONEL alloy 740 during creep.* Scripta Materialia, 2004. 51(6): p. 503-507.

[3] Sanders, J.M., et al., *Elimination of Fissures in Thick Section Inconel Alloy 740 Welds*, in *34th International Conference on Clean Coal & Fuel Systems*. 2009: Clearwater, FL.

[4] Shingledecker, J.P., N.D. Evans, and G.M. Pharr, *Influences of Composition and Grain Size on Creep-Rupture Behavior of Inconel Alloy 740.* Journal of Materials Engineering and Performance, 2012: p. *in review*.

[5] Shingledecker, J.P. and G.M. Pharr, *The Role of Eta Phase Formation on the Creep Strength and Ductility of Inconel Alloy 740 at 1023 K (750 C).* Metallurgical and Materials Transactions A, 2012: p. 10.1007/s11661-011-1013-4.

[6] Smith, G.D., B.A. Baker, and L.E. Shoemaker, *The Development of Inconel Alloy 740 for use as Superheater Tubing in Coal Fired Ultra Supercritical Boilers*, in *4th Annual Conference on Advances in Materials Technology for Fossil Power Plants*. 2004, Special Metals Corporation: Hilton Head, VA.

[7] Tung, D.C. and J.C. Lippold, *Weld Solidification Behavior of Ni-Base Superalloys for Use in Advanced Supercritical Coal-Fired Power Plants*, in *Superalloys 2012*, E.S. Huron, et al., Editors. 2012, TMS: Champion, PA. p. 563 - 567.

[8] Xie, X.S., et al., *A New Improvement of Inconel Alloy 740 for Usc Power Plants.* Advances in Materials Technology for Fossil Power Plants, 2008: p. 220-230.

[9] Zhao, S.Q., et al., *Research and Improvement on Structure Stability and Corrosion Resistance of Nickel-Base Superalloy INCONEL Alloy 740.* Materials & Design, 2006. 27(10): p. 1120-1127.

[10] Zhao, S.Q., et al., *Microstructural stability and mechanical properties of a new nickelbased superalloy.* Materials Science and Engineering a-Structural Materials Properties Microstructure and Processing, 2003. 355(1-2): p. 96-105.

[11] Bechetti, D.H., *Microstructural Evolution and Creep Rupture Behavior of Inconel Alloy 740H Fusion Welds*, in *Materials Science and Engineering*. M.S. Thesis. 2013, Lehigh University.
[12] Bader, M. *Investigation of Behaviour of Alloy 617mod*. in *Energy Day*. 2010. Rome.
[13] Hossain, S., C.E. Truman, and D.J. Smith, *Generation of Residual Stress and Plastic Strain in Fracture Mechanics Specimen to Study the Formation of Creep Damage in Type 316 Stainless Steel.* Fatigue and Fracture of Engineering Materials and Structures, 2011. 34: p. 654-666.
[14] Siefert, J.A. and J.M. Tanzosh, *Stress Relaxation Cracking Literature Review.* EPRI Conference Paper.
[15] Turski, M., et al., *Residual Stress Driven Creep Cracking in AISI Type 316H Stainless Steel.* Acta Materialia, 2008. 56: p. 3598-3612.
[16] Lippold, J.C. and D.J. Kotecki, *Weldability and Welding Metallurgy of Stainless Steels*. 2005, Hoboken, N.J.: John Wiley & Sons.
[17] Van Wortel, J.C., *Prevention of Relaxation Cracking by Material Selection and/or Heat Treatment Final Report*. 2000, TNO.
[18] Dhooge, A. and A. Vinckier, *Reheat Cracking - Review of Recent Studies (1984-1990).* Welding in the World, 1992. 30: p. 44-71.
[19] Spindler, M.W., *The Use of Borland Specimens to Reproduce Reheat Cracking in Type 316H*, in *Int. Conf. on High Temperature Plant Integrity and Life Extension*. 2004: Robinson College, Cambridge University.
[20] *Abaqus Software*. 2012, Dassault Systemes Simulia Corp.: Providence, R.I.
[21] *Inconel Alloy 800 Technical Bulletin*. 2004, Special Metals.
[22] *Inconel Alloy 617 Technical Bulletin*. 2005, Special Metals.
[23] *Inconel Alloy 740 Technical Bulletin*. 2004, Special Metals.
[24] *Abaqus v6.12 Analysis User's Manual Vol. 1: Introduction, Spatial Modeling, Execution & Output*. 2012, Providence, R.I.
[25] Whittaker, M.T., M. Evans, and B. Wilshire, *Long-Term Creep Data Prediction for Type 316H Stainless Steel.* Materials Science and Engineering A, 2012. 552: p. 145-150.